Grain-level residual stress distribution at dwell fatigue crack tips in a nickel-based superalloy

Joris Everaerts [a,b], Hangyue Li [c], Wei Li [d], Alexander M. Korsunsky [a]

[a] Department of Engineering Science, University of Oxford, Oxford, OX1 3PJ, UK

[b] Current affiliation: Department of Materials Engineering, KU Leuven, Kasteelpark Arenberg 44 bus 2450, 3001 Leuven, Belgium

[c] School of Metallurgy and Materials, University of Birmingham, Birmingham, B15 2TT, UK

[d] Rolls-Royce plc, Elton Road, Derby, DE24 8ED, UK

Abstract

Dwell fatigue crack growth in nickel-based superalloys is influenced by a complex interplay between mechanical and chemical phenomena. The stress distribution at the crack tip is closely related to these phenomena and to the local microstructure. In this study we evaluate experimentally the microscale residual stress distribution ahead of crack tips in RR1000 alloy samples after interrupted high temperature dwell fatigue testing. In the crack opening direction the results show a compressive residual stress zone, the extent of which is linked to the plastic zone size and crack growth retardation behaviour. In the direction of crack propagation the residual stress is also influenced by crystallographic grain orientation. The results demonstrate a novel approach of experimentally evaluating crack tip stress distribution via focused ion beam – digital image correlation (FIB-DIC) ring-core measurements at the grain-level. This provides new insights into fatigue crack growth in microstructurally heterogeneous materials.

Keywords: fatigue; creep; residual stresses; superalloy; focused ion beam (FIB)

A key requirement for nickel-based superalloys in turbine disc applications is resistance to crack growth during dwell fatigue, i.e. periodic sustained loading. Dwell fatigue crack growth resistance is affected by several interacting mechanisms. Creep damage can cause accelerated crack growth due to the formation of cavities at grain boundaries [1]. Plastic creep deformation can lead to stress relaxation, which lowers the stress ahead of the crack tip and hence results in crack growth retardation [2,3]. Besides creep effects, the high operating temperatures and oxidizing environment also affect crack growth rates. Formation of complex oxides can occur at the crack tip, thereby lowering the local fracture toughness, as well as ahead of the crack tip along grain boundaries under tensile stress, which is known as stress assisted grain boundary oxidation [4–7]. Furthermore, oxide formation presumably results in an alteration of the local stress field [8,9]. Oxidation and microscale stresses are thus interacting with each other. Given that both creep and oxidation are time-dependent phenomena, it is not surprising that sustained loading results in different and generally higher crack growth rates than what is observed during fatigue without dwell cycles [10,11].

Despite extensive research on the dwell fatigue resistance of Ni superalloys, knowledge regarding the complex stress distribution ahead of such cracks is limited. A micromechanical model by Chan et al. predicted a zone of compressive stress, which could shield the tensile stresses at the crack tip [12]. In contrast, a model by Cimbaro et al. which assumed the presence of a triangular oxide inclusion at the crack tip showed an anti-shielding effect, i.e. an additional tensile load at the crack tip due to the misfit strain of the oxide, although creep was not taken into account [9]. The effect of load and temperature on stress relaxation and the stress distribution at the crack tip was also examined via finite element modelling, illustrating the link with environmental degradation [13,14]. It is important to note that all of these observations are based on theoretical models.

In general it is very challenging to experimentally determine the microscale stress distribution ahead of crack tips, especially if the crack is growing through a microstructurally heterogeneous material. Additionally, classical fracture mechanics theories typically assume that the material is a homogeneous continuum. In the case of dwell fatigue in Ni superalloys the local microstructure could have a significant impact on creep relaxation, grain-level stress distribution, and thus crack growth rate. In this study, we demonstrate that it is possible to examine experimentally the influence of microstructure on the grain-level stress distribution in front of cracks, by evaluating the residual stress field ahead of crack tips on cross-sections of nickel-based superalloy samples subjected to interrupted dwell fatigue crack growth tests.

In a previous study [15], corner notched samples were produced from coarse-grained alloy RR1000 after super-solvus solution annealing (2 hours at 1170 °C) followed by ageing (16 hours at 760 °C). The nominal composition of this alloy in wt.% is 52.3 Ni, 18.5 Co, 15 Cr, 5 Mo, 3.6 Ti, 3 Al, 2 Ta, 0.5 Hf, 0.06 Zr, 0.027 C and 0.015 B [16]. After solution annealing, one group of samples was fast cooled (FC) at a rate of 1.8 °C/s and the other group was slow cooled (SC) at 0.7 °C/s in order to alter precipitation of the γ' phase [17]. The corner notched samples, which have a square cross-section of 7 x 7 mm^2, were tested in air at 700 °C with peak stress 482 MPa and a load ratio of 0.1. The fatigue tests were conducted using two alternating blocks of trapezoidal loading waveform: (a) baseline fatigue loading with a 1 s hold at peak load (1-1-1-1) and (b) with a long dwell period (3600 s) at peak load (1-3600-1-1). The durations for load ramp-up, ramp-down and holding at the minimum load were all set at 1 s for both loading waveforms. Figure 1 illustrates the different dwell fatigue crack growth behaviour of FC and SC samples, with the SC samples showing pronounced crack growth retardation during the first segment of dwell fatigue cycles within a ΔK range of 20-25 MPa√m. This difference was attributed to the different morphology and size distribution of secondary γ' precipitates in both samples, as observed on high resolution images that can be found in Ref. [15].

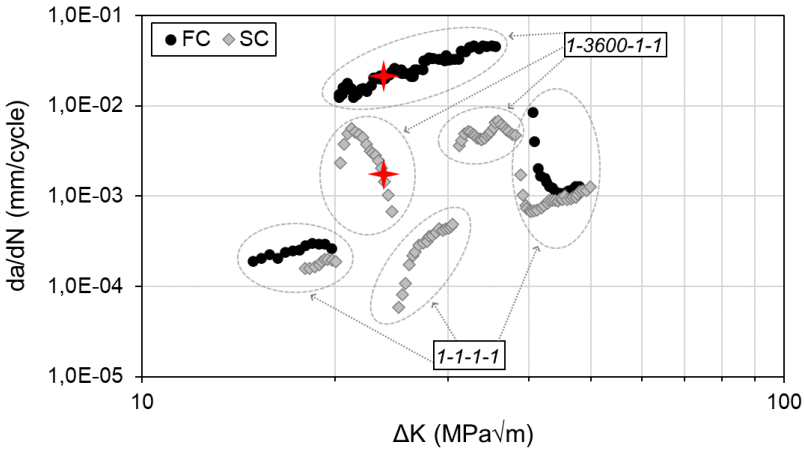

Figure 1. Dwell fatigue crack growth resistance (da/dN versus ΔK) curves for FC and SC samples as measured in a previous study [15] with alternating blocks of baseline (1-1-1-1) and dwell (1-3600-1-1) fatigue loading. Red crosses indicate the point of interruption for the two samples in the present study.

The dwell fatigue tests of one SC and one FC sample were interrupted during the first block of dwell fatigue cycles at a stress intensity factor range (*ΔK*) of 23.6 MPa√m (red crosses in Figure 1) for further examination in the current study. The two samples were cut along the diagonal plane to obtain a cross-section through the crack (Figure 2), and then electrochemically polished for 5 minutes with current density 50 A/dm^2 in an electrolyte containing 20 vol.% H_2SO_4 in absolute methanol in order to avoid polishing-induced surface stress [18]. Scanning electron microscopy (SEM) and focused ion beam (FIB) milling was

performed with a Tescan LYRA3 FIB-SEM microscope equipped with Oxford Instruments NordlysNano detector for electron backscatter diffraction (EBSD) measurements.

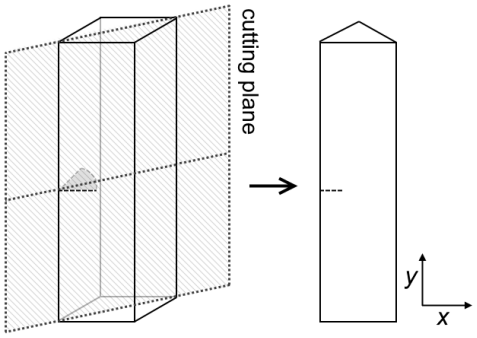

Figure 2. Illustration of diagonal cross-section through corner notched samples, with x the macroscopic crack growth direction and y the loading direction

FIB-DIC ring-core measurements were performed in both samples in order to examine the residual stress distribution in front of the cracks. In this technique, an annulus is machined incrementally by FIB milling, thereby forming a central ring-core or micropillar, whilst the top surface of the pillar is imaged by scanning electron microscopy (SEM). If a stress is present in the material, DIC analysis of the SEM images will show a gradual strain relief in the material due to progressive milling. In the current study, ring-cores with diameter 5 μm were milled in 40 steps of 125 nm depth, with FIB parameters 30 keV and 0.17 nA. Ten SEM images were acquired in between each milling step with a resolution of 1250x1250 pixels. Stopping the process at a milling depth equal to the ring-core diameter (5 μm) ensures complete strain relief within the micropillar [19]. A thin Pt coating was applied to the samples prior to these measurements, which after two FIB scanning passes formed a pattern suitable for DIC [20]. Strain relief data from DIC analysis were averaged for the ten SEM images obtained after each milling step to reduce noise. The relief strain that was measured after each milling step was fitted to a master profile obtained from FE modelling as described in Ref. [19], to determine the total in-plane relief strain values parallel (*x* direction) and perpendicular (*y* direction) to the macroscopic crack growth direction. The residual stress values were determined via Hooke's law using a tensor calculation by means of a Mathematica notebook [21], which accounts for crystallographic anisotropy. The Euler angles of each specific grain in which a FIB-DIC ring-core measurement was located were obtained by EBSD and used as input for this calculation, as well as the single crystal elastic stiffness coefficients measured for alloy RR1000 [22]. Finally, the estimated error for the ring-core FIB-DIC measurements was calculated based on the work of Lunt & Korsunsky [23] and takes into account the error observed during DIC analysis and the error caused by fitting the relief strain data to the master relief curve. Note that all error bars for FIB-DIC ring-core data in this study represent a 95% confidence interval.

High magnification SEM images near the crack tip in both the fast cooled (FC) and slow cooled (SC) sample are shown in Figure 3. Note that the crack in the FC sample has locally deflected away from the macroscopic crack growth direction, which is the x direction. The darker contrast in the crack wake behind both crack tips indicates the presence of a thin sub-micron oxide layer, which was examined in more detail in Ref. [15] and consists of Ni, Co, Cr and Al oxides. The oxide is known to intrude a few microns into the grain boundary in front of the crack tip [15], which makes it difficult to pinpoint the exact crack tip location in the secondary electron images in Figure 3. The electrochemical polishing used during sample preparation reveals the γ' precipitate structure in both samples. The contrast between γ matrix and γ' phase indicates that the γ' phase was removed at a slightly higher rate than the γ matrix. Finally, the image of the SC sample shows an altered γ' precipitate structure along the grain boundary ahead of the crack tip, with a few coarser precipitates (indicated by arrows). This phenomenon of selective γ' coarsening by local dissolution of fine, tertiary γ' was also observed by Knowles & Hunt [24], who argue that this results in alloy softening and thus local stress relaxation.

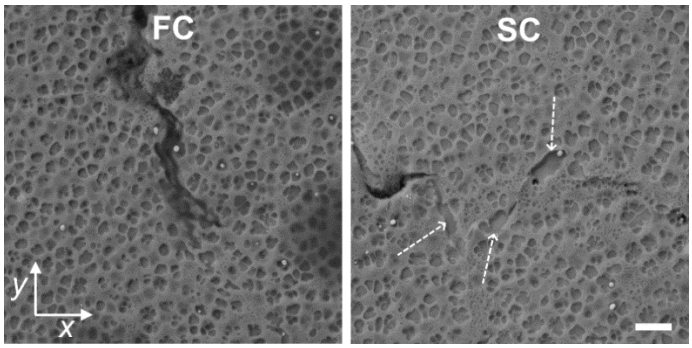

Figure 3. SEM images near the crack tip in the fast cooled (FC) and slow cooled (SC) sample, with x the macroscopic crack growth direction and y the loading direction (scale bar 1 μm).

The residual stress distribution ahead of the crack tips was evaluated via a series of FIB-DIC ring-core measurements. These measurements are visible in Figure 4, which shows lower magnification SEM images of the regions in front of the crack tip in both samples, overlaid with inverse pole figure maps to illustrate grain orientations. The grain size is relatively large for both samples, with the mean equivalent area grain diameter approximately 49 μm as determined in a previous study [15]. The FIB-DIC ring-core measurements, with core diameter 5 μm, are clearly much smaller than the grain size, which means that they are sensitive to inter- and intragranular residual stress variation [20]. The crack in the SC sample is seen to be growing along a grain boundary in a direction that is close to the macroscopic crack growth

direction (x), while the crack in FC sample has bifurcated around a grain, with both crack paths deflected more towards the loading axis (y).

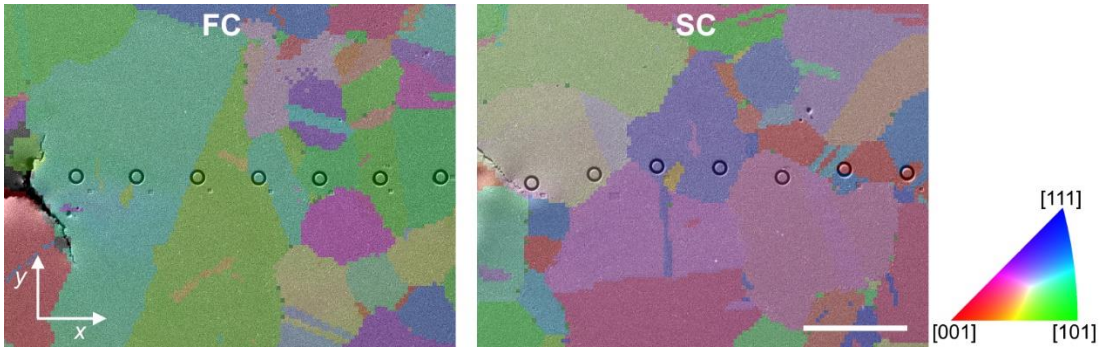

Figure 4. SEM images with overlay of inverse pole figure map (reference direction y) of area in front of crack tips in the fast cooled (FC) and slow cooled (SC) sample, also showing the FIB-DIC ring-core measurements (scale bar 50 µm)

The results of the FIB-DIC measurements are presented in Figure 5. For both samples, the residual stress in the loading direction (Figure 5a) is compressive, with values close to the yield stress of approximately 900 MPa near the crack tip [25]. The stress magnitude in the FC sample decreases rapidly and almost linearly with distance from the crack tip, reaching nearly zero at a distance of 180 µm. In the SC sample, however, the compressive zone extends deeper into the material in front of the crack tip. Note that for this sample three additional measurements were performed, which are not shown in Figure 4, confirming that the residual stress remains compressive at a distance of at least 270 µm from the crack tip. These results are in agreement with the crack growth rate data (Figure 1), which show pronounced crack growth retardation for the SC sample, with a growth rate approximately 24 times slower than the FC sample at the point of interruption (ΔK=23.6 MPa√m). This indicates the presence of a larger creep zone in the SC sample, presumably due to the difference in morphology and size distribution of γ' precipitates in both samples, which is known to affect creep and plastic deformation [26,27]. This extended creep zone logically results in an extended zone of residual compressive stress after unloading, as observed in Figure 5a. For the SC sample, the crack growth rate (Figure 1) after the first block of dwell fatigue cycles returns to fatigue baseline rates at a ΔK value of roughly 25.5 MPa√m after growing below this baseline for some distance. This can be used for a first estimation of the extent of the creep zone in this sample. The average crack length a depends on ΔK as:

$$a = \frac{1}{\pi}\left(\frac{\Delta K}{Y\Delta\sigma}\right)^2$$

with Y a geometric factor equal to 0.708 at the centre of a corner crack [28], and $\Delta\sigma$ the stress range (in this case equal to 433.8 MPa). At the point of interruption (ΔK=23.6 MPa√m, Figure

4) the crack length is about 1.88 mm. Crack growth reaches fatigue baselines rates again at a crack length of 2.19 mm (at $\Delta K \approx 25.5$ MPa$\sqrt{m}$). The difference of 310 µm is an estimate of the extent of the creep zone that is present in the SC sample. i.e. the zone through which the crack growth rate after the dwell cycle is reduced. Therefore, as plastic deformation cannot be recovered, at 270 µm from the crack tip the residual stress in the crack opening direction would indeed be expected to still be compressive after unloading. This is exactly the case with the measured results, as shown in Figure 5a. The residual stress in the crack growth direction, however, is complex for both samples and does not show a clear dependency on the distance from the crack tip (Figure 5b). However, comparison with Figure 4 indicates a potential link with crystallographic orientation. For example, the first two data points for the SC sample have comparable values and were also measured within the same grain. This is the case for data points three and four as well, and similar observations can be made for the FC sample.

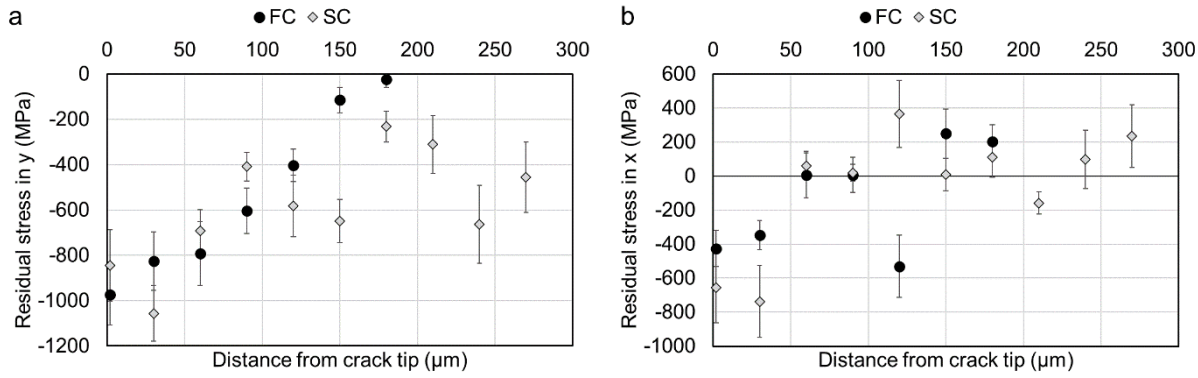

Figure 5. Residual stress obtained via FIB-DIC ring-core measurements ahead of crack tips in the fast cooled (FC) and slow cooled (SC) sample: a) in the loading i.e. crack opening (y) direction and b) in the macroscopic crack growth (x) direction.

In general for all data (both in *x* and *y*), it is not observed that the stress is inversely proportional to the square root of the distance from the crack tip, as prescribed by fracture mechanics. This can be understood firstly by the occurrence of creep relaxation and secondly by the heterogeneity of the material at the microscale, i.e. the grain structure, which is not accounted for in classical fracture mechanics theories. However, it should be noted that the current study contains a few limitations. First, the temperature during dwell fatigue testing was 700 °C, but the residual stress distribution was analysed at room temperature after test interruption. Cooling could have affected the grain-level stresses due to anisotropic thermal expansion. It is thus difficult to directly extrapolate the results to the crack tip stress distribution in samples under load at 700 °C. Second, the effect of the submicron oxide layer on crack tip stress could not be measured via the FIB-DIC technique due to its limited spatial resolution. Third, by sectioning through the cracks the stress distribution could have been altered. Assuming that grain-level stresses at crack tips are tensorial, this effect should be assessed in future studies,

for example via serial sectioning combined with 3D crystal plasticity simulations. Finally, the influence of crack bifurcation on stress distribution was not investigated, but could be examined in more detail in future research as well.

Nonetheless, it is clear that the experimental methodology of grain-level residual stress evaluation ahead of crack tips presented in this work is highly promising to study the effect of local microstructure on crack growth and fracture, not only for the specific case of dwell fatigue in Ni superalloys but for a wide range of materials and load cases.

In summary, grain-level residual stresses ahead of crack tips in nickel-based superalloy samples were evaluated experimentally via FIB-DIC ring-core measurements in order to gain insights into dwell fatigue crack growth resistance. In the coarse-grained RR1000 alloy samples, which were subjected to interrupted dwell fatigue tests, a zone of compressive residual stress was observed in the crack opening direction. This zone corresponds to a creep zone, the extent of which can be linked to crack growth retardation. The residual stress in the crack growth direction showed strong variation from grain to grain. These results indicate that the complex stress distribution at crack tips due to microstructural heterogeneity can be evaluated experimentally using the FIB-DIC technique, which opens up new possibilities for studying the influence of microstructure on crack growth.

Acknowledgements

The authors would like to acknowledge Rolls-Royce plc for the funding support.

References

[1] D.M. Knowles, D.K. Skelton, High temperature fatigue of a polycrystalline nickel base superalloy, Mater. Sci. Technol. 17 (2001) 1403–1412. https://doi.org/10.1179/026708301101509377.

[2] Y.J. Oh, J.H. Hong, A model for creep-fatigue interaction in terms of crack-tip stress relaxation, Metall. Mater. Trans. A. 31 (2000) 1761–1775. https://doi.org/10.1007/s11661-998-0327-3.

[3] X. Liu, B. Kang, K.M. Chang, The effect of hold-time on fatigue crack growth behaviors of WASPALOY alloy at elevated temperature, Mater. Sci. Eng. A. 340 (2003) 8–14. https://doi.org/10.1016/S0921-5093(02)00074-6.

[4] S. Cruchley, H.Y. Li, H.E. Evans, P. Bowen, D.J. Child, M.C. Hardy, The role of oxidation damage in fatigue crack initiation of an advanced Ni-based superalloy, Int. J. Fatigue. 81 (2015) 265–274. https://doi.org/10.1016/j.ijfatigue.2015.08.016.

[5] H.S. Kitaguchi, H.Y. Li, H.E. Evans, R.G. Ding, I.P. Jones, G. Baxter, P. Bowen, Oxidation ahead of a crack tip in an advanced Ni-based superalloy, Acta Mater. 61 (2013) 1968–1981. https://doi.org/10.1016/j.actamat.2012.12.017.

[6] R. Jiang, P.A.S. Reed, Critical Assessment 21: oxygen-assisted fatigue crack propagation in turbine disc superalloys, Mater. Sci. Technol. 32 (2016) 401–406. https://doi.org/10.1080/02670836.2016.1148227.

[7] G.B. Viswanathan, D.E. Mills, M.J. Mills, Oxidation-Related Microstructural Changes at a Crack Tip in Waspaloy After Elevated-Temperature Dwell-Fatigue Testing, Metall Mater Trans A. 50 (2019) 5574–5580. https://doi.org/10.1007/s11661-019-05499-0.

[8] J. Everaerts, E. Salvati, H. Li, W. Li, A.M. Korsunsky, Mechanical properties of thermally grown submicron oxide layers on a nickel-based superalloy, Corros. Sci. 165 (2020). https://doi.org/10.1016/j.corsci.2019.108388.

[9] L. Cimbaro, A.P. Sutton, D.S. Balint, A.T. Paxton, M.C. Hardy, Embrittlement of an elasto-plastic medium by an inclusion, Int. J. Fract. (2019). https://doi.org/10.1007/s10704-019-00344-2.

[10] E. Andrieu, R. Molins, H. Ghonem, A. Pineau, Intergranular crack tip oxidation mechanism in a nickel-based superalloy, Mater. Sci. Eng. A. 154 (1992) 21–28. https://doi.org/10.1016/0921-5093(92)90358-8.

[11] J. Byrne, R. Hall, L. Grabowski, Elevated temperature fatigue crack growth under dwell conditions in Waspaloy, Int. J. Fatigue. 19 (1997) 359–367. https://doi.org/10.1016/S0142-1123(97)00056-X.

[12] K.S. Chan, Time-Dependent Crack Growth Thresholds of Ni-Base Superalloys, Metall. Mater. Trans. A. 45 (2014) 3454–3466. https://doi.org/10.1007/s11661-014-2271-8.

[13] A. Pineau, S.D. Antolovich, High temperature fatigue of nickel-base superalloys – A review with special emphasis on deformation modes and oxidation, Eng. Fail. Anal. 16 (2009) 2668–2697. https://doi.org/10.1016/j.engfailanal.2009.01.010.

[14] S. Ponnelle, B. Brethes, A. Pineau, Propagation des fissures par fatigue dans les disques de turbine en Inconel 718 : effets de la microstructure et de chargements complexes, J. Phys. IV France. 10 (2000) Pr4-277-Pr4-282. https://doi.org/10.1051/jp4:2000439.

[15] H.Y. Li, J.F. Sun, M.C. Hardy, H.E. Evans, S.J. Williams, T.J.A. Doel, P. Bowen, Effects of microstructure on high temperature dwell fatigue crack growth in a coarse grain PM nickel based superalloy, Acta Mater. 90 (2015) 355–369. https://doi.org/10.1016/j.actamat.2015.02.023.

[16] S.J. Hessel, W. Voice, A.W. James, S.A. Blackham, C.J. Small, M.R. Winstone, Nickel Alloy for Turbine Engine Component, EP0803585A1, 2000.

[17] R.C. Reed, The Superalloys: fundamentals and applications, Cambridge University Press, 2006. https://doi.org/10.1017/CBO9780511541285.

[18] J. Everaerts, E. Salvati, A.M. Korsunsky, Nanoscale Depth Profiling of Residual Stresses Due to Fine Surface Finishing, Adv. Mater. Interfaces. 6 (2019) 1900947. https://doi.org/10.1002/admi.201900947.

[19] A.M. Korsunsky, M. Sebastiani, E. Bemporad, Residual stress evaluation at the micrometer scale: Analysis of thin coatings by FIB milling and digital image correlation, Surf. Coat. Technol. 205 (2010) 2393–2403. https://doi.org/10.1016/j.surfcoat.2010.09.033.
[20] J. Everaerts, X. Song, B. Nagarajan, A.M. Korsunsky, Evaluation of macro- and microscopic residual stresses in laser shock-peened titanium alloy by FIB-DIC ring-core milling with different core diameters, Surf. Coat. Technol. 349 (2018) 719–724. https://doi.org/10.1016/j.surfcoat.2018.06.043.
[21] E. Salvati, T. Sui, A.M. Korsunsky, Uncertainty quantification of residual stress evaluation by the FIB-DIC ring-core method due to elastic anisotropy effects, Int. J. Solids Struct. 87 (2016) 61–69. https://doi.org/10.1016/j.ijsolstr.2016.02.031.
[22] J. Everaerts, C. Papadaki, W. Li, A.M. Korsunsky, Evaluation of single crystal elastic stiffness coefficients of a nickel-based superalloy by electron backscatter diffraction and nanoindentation, J. Mech. Phys. Solids. 131 (2019). https://doi.org/10.1016/j.jmps.2019.07.011.
[23] A.J.G. Lunt, A.M. Korsunsky, A review of micro-scale focused ion beam milling and digital image correlation analysis for residual stress evaluation and error estimation, Surf. Coat. Technol. 283 (2015) 373–388. https://doi.org/10.1016/J.SURFCOAT.2015.10.049.
[24] D.M. Knowles, D.W. Hunt, The influence of microstructure and environment on the crack growth behavior of powder metallurgy nickel superalloy RR1000, Metall and Mat Trans A. 33 (2002) 3165–3172. https://doi.org/10.1007/s11661-002-0302-3.
[25] N.G. Jones, K.A. Christofidou, P.M. Mignanelli, J.P. Minshull, M.C. Hardy, H.J. Stone, Influence of elevated Co and Ti levels on polycrystalline powder processed Ni-base superalloy, Mater. Sci. Technol. 30 (2014) 1853–1861. https://doi.org/10.1179/1743284714Y.0000000509.
[26] B. Engel, J.P. Rouse, C.J. Hyde, W. Lavie, D. Leidermark, S. Stekovic, S.J. Williams, S.J. Pattison, B. Grant, M.T. Whittaker, J.P. Jones, R.J. Lancaster, H.Y. Li, The prediction of crack propagation in coarse grain RR1000 using a unified modelling approach, Int. J. Fatigue. 137 (2020) 105652. https://doi.org/10.1016/j.ijfatigue.2020.105652.
[27] J. Telesman, P. Kantzos, J. Gayda, P.J. Bonacuse, A. Prescenzi, Microstructural Variables Controlling Time-Dependent Crack Growth in a P/M Superalloy, in: Superalloys 2004 (Tenth International Symposium), TMS, 2004: pp. 215–224. https://doi.org/10.7449/2004/Superalloys_2004_215_224.
[28] H. Tada, P.C. Paris, G.R. Irwin, The stress analysis of cracks handbook, 3rd ed, ASME Press, New York, 2000.